

Thermoresponsive and Photocrosslinkable Poly(2-alkyl-2-oxazoline) Toolbox – Customizable Ultralow-Fouling Hydrogel Coatings for Blood Plasma Environments

Fiona Wiesner (née Diehl), Christian Petri, Simone Hageneder, Cleiton Kunzler, Sven Klees, Petra Frank, Matthias Pertiller, Jakub Dostalek, Wolfgang Knoll, and Ulrich Jonas*

This study focuses on developing surface coatings with excellent antifouling properties, crucial for applications in the medical, biological, and technical fields, for materials and devices in direct contact with living tissues and bodily fluids such as blood. This approach combines thermoresponsive poly(2-alkyl-2-oxazoline)s, known for their inherent protein-repellent characteristics, with established antifouling motifs based on betaines. The polymer framework is constructed from various monomer types, including a novel benzophenone-modified 2-oxazoline for photocrosslinking and an azide-functionalized 2-oxazoline, allowing subsequent modification with alkyne-substituted antifouling motifs through copper(I)-catalyzed azide-alkyne cycloaddition. From these polymers surface-attached networks are created on benzophenone-modified gold substrates via photocrosslinking, resulting in hydrogel coatings with several micrometers thickness when swollen with aqueous media. Given that poly(2-alkyl-2-oxazoline)s can exhibit a lower critical solution temperature in water, their temperature-dependent solubility is compared to the swelling behavior of the surface-attached hydrogels upon thermal stimulation. The antifouling performance of these hydrogel coatings in contact with human blood plasma is further evaluated by surface plasmon resonance and optical waveguide spectroscopy. All surfaces demonstrate extremely low retention of blood plasma components, even with undiluted plasma. Notably, hydrogel layers with sulfobetaine moieties allow efficient penetration by plasma components, which can then be easily removed by rinsing with buffer.

1. Introduction

Antifouling substrate and surface materials, which protect an object from nonspecific adsorption of biomolecular entities and subsequent growth of biofilms, have gained critical importance in such versatile fields of science, like biomedicine (e.g. as coatings for medical devices and implants, such as urinal and breathing catheters, feeding tubes, injection equipment, temporary implants, blood filtration, to mention a few),^[1] marine engineering (e.g. as coatings for ship bodies to improve their hydrodynamics and minimize their drag),^[2] and sensor technologies (e.g. as protection layer for sensor transducers in contact with body fluids).^[3,4] A particular challenge and demand presents the availability of surface coatings, which exhibit essentially no protein adsorption upon contact with human blood plasma (HBP) or whole blood. In the literature, a plethora of antifouling compounds has been developed and investigated,^[5] with the most prominent examples comprising poly(ethylene glycol)/oligo(ethylene glycol) (PEG/OEG),^[6] zwitterionic polymers,^[7] and polysaccharide-based materials.^[8] The

F. Wiesner (née Diehl), C. Petri, C. Kunzler, S. Klees, P. Frank, U. Jonas
 Macromolecular Chemistry
 Department Chemistry-Biology
 University of Siegen
 Adolf-Reichwein-Strasse 2, 57076 Siegen, Germany
 E-mail: jonas@chemie.uni-siegen.de

 The ORCID identification number(s) for the author(s) of this article can be found under <https://doi.org/10.1002/marc.202300549>

© 2023 The Authors. Macromolecular Rapid Communications published by Wiley-VCH GmbH. This is an open access article under the terms of the Creative Commons Attribution License, which permits use, distribution and reproduction in any medium, provided the original work is properly cited.

DOI: 10.1002/marc.202300549

S. Hageneder, M. Pertiller, J. Dostalek, W. Knoll
 Biosensor Technologies
 AIT-Austrian Institute of Technology GmbH
 Konrad-Lorenz-Straße 24, Tulln an der Donau 3430, Austria
 J. Dostalek
 FZU-Institute of Physics
 Czech Academy of Sciences
 Na Slovance 2, Prague 182 21, Czech Republic
 J. Dostalek, W. Knoll
 Laboratory for Life Sciences and Technology (LiST)
 Danube Private University
 Konrad-Lorenz-Straße 24, Tulln an der Donau 3430, Austria

commonly accepted working principle of antifouling coatings implies the formation of a tightly bound water layer on the surface that hinders proteins and other biological entities to adsorb.^[5] Consequently, a strong hydrophilicity for association of water molecules to the surface presents the main requirement identified for effective antifouling motifs. For ionic and zwitterionic compounds, the effectiveness to bind the hydrate layer is enhanced by electrostatic interactions, providing further resistance to protein adsorption.^[9,10] Many procedures to increase the surface hydrophilicity, like anodization for metals and plasma treatments of conductive and non-conductive surfaces,^[11] result in rather transient surface modification, while deposition of self-assembled monolayers (SAMs), polymer brushes, and hydrogel coatings often yield permanent effects. For the latter cases of surface-attached molecular entities, physicochemical characteristics, such as polymer chain flexibility, packing density, molecular mass, and surface charge, are crucial for potent antifouling qualities.^[12,13]

A particular interesting class of powerful antifouling materials are polymer network-based hydrogels, which can retain substantial amounts of water due to the hydrophilic nature of the underlying polymer backbone. Such water-swollen polymer networks are held together either by physical or chemical crosslinks between the polymer chains, rendering the material insoluble and maintaining its structural integrity over extended periods of time, especially in the case of covalent crosslinks. The counteracting effects of the osmotic pressure of water hydrating the polymer segments, which leads to an expansive force, and the entropically driven tendency of the flexible chain segments to coil into a random conformation, inducing a contracting force, result in the equilibrium swelling state of the network.

Methods for chemical crosslinking entail 1) *in situ* crosslinking during polymerization and 2) post-polymerization crosslinking by external stimuli, such as UV light (photocrosslinking),^[14–17] or temperature increase (thermal crosslinking).^[18,19] In particular, the post-polymerization photocrosslinking technique enables the simultaneous preparation of ultra-thin polymer network coatings and covalent attachment to an organic surface material. Inorganic surfaces, like gold metal, may be pre-treated with an adhesion promoting layer bearing for example, benzophenone moieties in order to endow the substrate with photocrosslinking entities.

The potential of poly(2-alkyl-2-oxazoline)s, investigated in the present work, lies in their renown anti-fouling capacities, to serve as base material in photocrosslinked hydrogel architectures that can be further enhanced by other antifouling motifs via a modular click chemistry approach. Poly(2-alkyl-2-oxazoline)s possess a pseudo-peptidic backbone structure and, in addition to their antifouling properties, are characterized by a pronounced biocompatibility.^[20,21] Depending on the specific alkyl substituent, they can also show a lower critical solution temperature (LCST) behavior in water, being hydrophilic and dissolved below the cloud point temperature, while undergoing rearrangement of the hydrogen-bonding arrangement with lower affinity of the polymer to water when heated above this point. This process ultimately results in phase separation into a polymer poor and a polymer rich fraction that eventually leads to polymer precipitation.^[22] Such volume transitions resulting from the LCST behavior have been exploited for reversible actuation in ad-

vanced biosensor applications and are particularly suitable for responsive binding matrices.^[23–29]

Poly(2-alkyl-2-oxazoline)s are prepared by cationic ring-opening polymerization (CROP), which allows control over the target molar mass while retaining a narrow mass dispersity, and enables the design of advanced polymer architectures via variation of the comonomer types and sequence. However, this preparation technique is sensitive toward nucleophilic substances or side groups and the cationic chain end can be easily terminated by those. Due to these inherent limitations, many functional monomer types including common crosslinker structures (e.g. based on thiol or amino groups) and antifouling motifs cannot be directly implemented in the CROP procedure. Yet, including a crosslinker functionality in the polymer backbone would provide convenient access to poly(2-oxazoline) network architectures, which are interesting for a variety of applications, such as surface coatings and sensor matrices.

In the field of surface coatings, the possibility to perform crosslinking via irradiation with UV light after deposition of the polymer on a respective substrate extends the radius of operation substantially. Preparation of photocrosslinked poly(2-alkyl-2-oxazoline) networks was successfully demonstrated employing thiol-ene coupling chemistry by incorporation of either unsaturated double bonds into the polyoxazoline scaffold,^[30,31] or photocleavable-protected thiol side chains for simultaneous deprotection and crosslinking.^[32] Furthermore, such networks could be also obtained from coumarin-modified poly(oxazoline)s via photodimerization upon UV irradiation.^[33,34] These strategies suffer from the disadvantage of requiring two mutually reactive units in close proximity to successfully attain crosslinking, which becomes less probable owing to the restricted polymer dynamics compared to small molecules in solution. An additional problem may be the susceptibility to oxidation of the free thiol group involved in the thiol-ene coupling reaction. A photocrosslinker unit that avoids the above-mentioned issues is the well-known benzophenone moiety, as it is stable in the absence of UV light and only needs adjacent C–H bonds as requirement for the crosslinking process. The benzophenone motif was already utilized for the surface attachment of several different types of polymers.^[15,35–37] For poly(2-alkyl-2-oxazoline)s, two generic methods for the preparation of substrate coatings via photoactivation of benzophenone groups are reported in the literature. The first strategy is based on substrate modification with respective benzophenone-containing silanes and subsequent polymer deposition followed by irradiation, which results in thin polymer layers of a few nanometers.^[35] The second approach relies on the modification of the amine groups in a partially hydrolyzed poly(2-alkyl-2-oxazoline) with photoreactive benzophenone substituents.^[38–40] Yet, in order to target a well-defined polymer architecture, incorporation of the benzophenone motif into an oxazoline monomer would provide full control over the composition of the comonomer feed during CROP and thereby the exact ratio of crosslinking sites along the polymer backbone. An early report of molecular frameworks that contain both a 2-oxazoline and a benzophenone structure was provided by Kappel et al.^[41] in the context of pharmaceutical applications, but without reference to 2-alkyl-2-oxazoline polymers. When attempting the synthesis of 2-[(4-phenylphenoxy)methyl]-2-oxazoline following this procedure, in our hands we could isolate only the tautomer

2-(4-benzoylphenoxymethylidene)-1,3-oxazolidine, which was not subjected to CROP. To circumvent the potential risk of tautomerization at the oxazoline ring, we report in the present manuscript the synthesis of a 2-oxazoline derivative with longer alkyl spacer connecting the benzophenone unit, and which is susceptible to copolymerization with other 2-alkyl-2-oxazolines via CROP.

Besides the direct copolymerization of oxazoline photocrosslinker monomers, the inclusion of specific functional groups into the poly(oxazoline) backbone, such as protic antifouling motifs, is difficult due to the sensitivity of CROP toward nucleophilic moieties. A versatile route to endow the polymer scaffold with functional substituents in a post-polymerization modification reaction is provided by azide click chemistry, which provides a toolbox for convenient and effective coupling of alkyne-containing motifs to the azide group. This strategy was exploited here by utilizing an azide-containing oxazoline as comonomer in CROP to yield azide-functionalized poly(2-alkyl-2-oxazolines).^[42] The polymer backbones with azide modification were conjugated with suitable antifouling motifs in a modular crafting approach to further enhance the antifouling quality and to target respective applications via appropriate click combinations. At this stage, the soluble polymers could be fully analyzed by the standard polymer characterization methods to assess the efficiency of the click modification, which is rather difficult for an insoluble polymer network. Once such polymers were converted into hydrogel coatings by photocrosslinking, their characteristic properties, such as a) layer thickness, b) thermoresponsivity, and c) antifouling properties, were investigated by surface plasmon resonance (SPR) spectroscopy combined with optical waveguide spectroscopy (OWS). Specifically, the antifouling efficacy was analyzed by variation of the refractive index and thickness in the SPR/OWS sensor environment before and after a contact with biological fluids.^[43]

2. Results and Discussion

In the following discussion, we describe the synthetic strategies for a family of photocrosslinkable poly(2-alkyl-2-oxazolines) with antifouling backbone and pendent antifouling motifs, employing three components that can be freely combined in a modular approach via CROP. These three components consist of i) the benzophenone-based photocrosslinker monomer 2-[3-(4-benzoylphenoxy)propyl]-4,5-dihydro-1,3-oxazole (BPOxa), ii) the main monomers 2-ethyl-2-oxazoline (EtOxa) and 2-*iso*-propyl-2-oxazoline (iPrOxa) as building blocks for a non-fouling and potentially thermoresponsive polymer backbone, and iii) the azide-based oxazoline monomer 2-(3-azidopropyl)-4,5-dihydro-1,3-oxazole (AzOxa) for click coupling of the antifouling motifs that carry alkyne functions. The alkyne click agents themselves are comprised of different structural elements of the carboxy alkyne 4-pentynoic acid (COOH) for subsequent bioligand coupling, or of literature-known antifouling motifs based on the carboxybetaine 3-[dimethyl(prop-2-yn-1-yl)ammonio]propanoate (CB) and the sulfobetaine 3-[dimethyl(prop-2-yn-1-yl)ammonio]propane-1-sulfonate (SB), as well as the OEG units 2-{2-[2-(prop-2-yn-1-yloxy)ethoxy]ethoxy}ethan-1-ol (OEG) and 3-{dimethyl[2-[2-(prop-2-yn-1-yloxy)ethoxy]ethyl]ammonio}propane-1-sulfonate (OEG-SB). These alkyne motifs are all freely interchangeable to

further expand the modular range of the click-modified polymer toolbox. We further analyze the thermal properties of the multi-component copolymers in aqueous solution by turbidimetry for cloud point determination. After conversion of these copolymers into crosslinked, surface-attached copolymer networks and swelling with water or phosphate-buffered saline (PBS) to form hydrogel coatings, the response of their swelling ratios to temperature changes is characterized by SPR spectroscopy. Furthermore, SPR analysis of the hydrogel coatings in direct contact with HBP was performed to quantify their antifouling efficacy to adumbrate the performance in an anticipated application of biomedical context.

2.1. Monomer Synthesis, Polymerization, and Polymer Modification with Antifouling Motifs

2.1.1. Photocrosslinker Monomer

A 2-oxazoline with a benzophenone unit connected via a methoxy linkage has been reported in the literature.^[48] In our hands, this synthesis procedure did not yield the expected oxazoline derivative 2-[4-benzoylphenoxy)methyl]-4,5-dihydro-1,3-oxazole (**u1** in Scheme S14, Supporting Information), but the tautomeric product 2-(4-benzoylphenoxymethylidene)-1,3-oxazolidine (**u2**), as discussed in detail in Chapter S17 (Supporting Information). To avoid potential problems with such tautomerism, we developed a synthesis route for BPOxa (**4**) with propylene spacer between the 2-oxazoline core and the benzophenone substituent (**Figure 1A**).

In a first step, 4-hydroxybenzophenone was coupled to ethyl-4-bromobutyrate in the presence of K_2CO_3 , followed by alkaline hydrolysis with NaOH of the respective ester to yield 4-(benzoylphenoxy)butanoic acid (**1**). The resulting carboxylic acid functionality was then transformed into the *N*-hydroxysuccinimide (NHS) active ester **2** by reaction with trifluoroacetic anhydride (TFAA) and NHS, followed by amidation with 2-chloroethylamine. The obtained 4-(4-benzoylphenoxy)-*N*-(2-chloroethyl)butanamide (**3**) was then heated in the presence of anhydrous K_2CO_3 , which induces a ring closure forming the final product BPOxa (**4**) with an overall yield of $\approx 65\%$.

2.1.2. Main Monomers

While the main monomer EtOxa (**6**) was commercially available, iPrOxa (**7**), and nPrOxa (**8**) were synthesized according to Witte and Seeliger.^[49] In short, the corresponding alkyl nitriles (butyronitrile and isobutyronitrile) were reacted with 2-aminoethanol and $Cd(OAc)_2$ as catalyst to form the 2-alkyl-oxazoline ring in yields above 65%.

2.1.3. Azide Monomer

The azide monomer 2-(3-azidopropyl)-4,5-dihydro-1,3-oxazole (AzOxa, **13**, see **Figure 2A**) was prepared in analogy to the literature, in which the synthesis of the phenyl derivative was described.^[50,51]

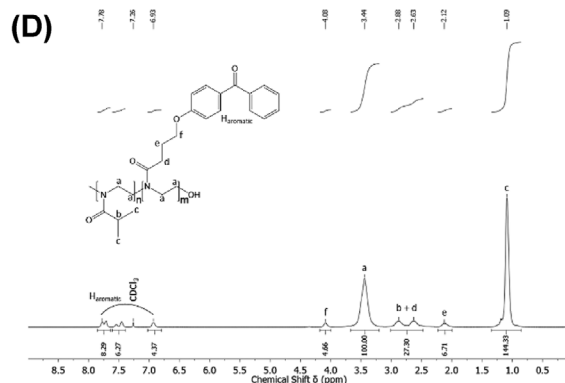
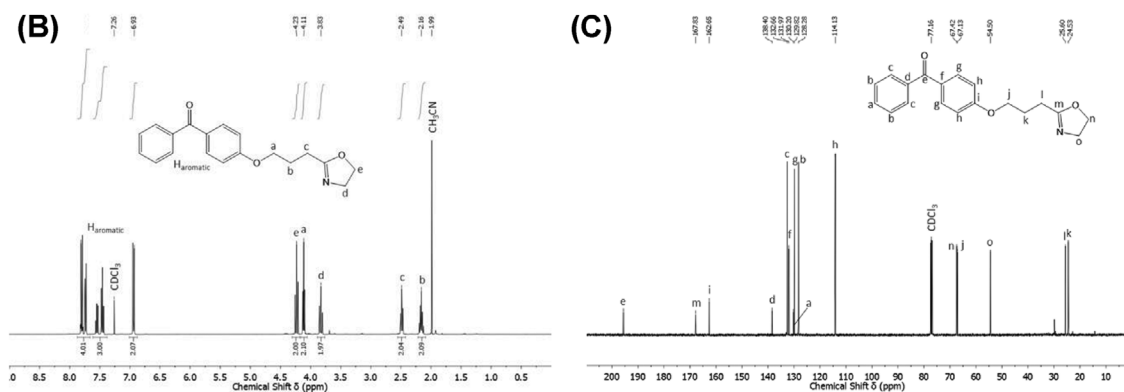
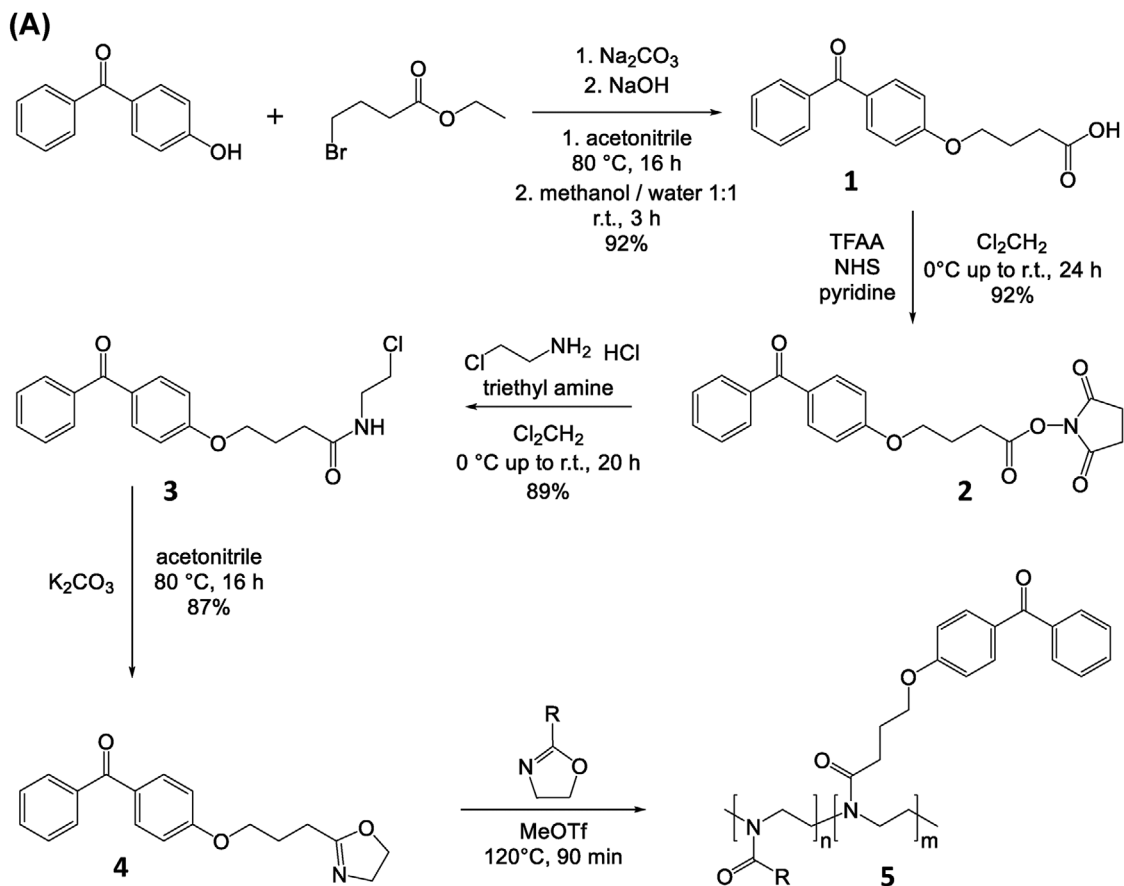


Figure 1. A) Synthesis route for 2-[3-(4-benzoylphenoxy)propyl]-4,5-dihydro-1,3-oxazole (BPOxa, **4**) and its copolymerization (NHS = *N*-hydroxysuccinimide, TFAA = trifluoroacetic anhydride, MeOTf = methyl trifluoromethanesulfonate). B) ^1H NMR spectrum of BPOxa (**4**) measured at r.t. in CDCl_3 (with a Larmor frequency of 400 MHz). C) ^{13}C NMR spectrum of BPOxa (**4**), measured at r.t. with 100 MHz in CDCl_3 . D) Representative ^1H NMR spectrum of poly(iPrOxa₉₄-co-BPOxa₆), measured at r.t. with 400 MHz in CDCl_3 .

In the first step, the bromine of ethyl-4-bromobutyrate was substituted by NaN_3 to yield ethyl-4-azidobutyrate (**9**), followed by alkaline hydrolysis of the ester leading to 4-azidobutanoic acid (**10**). The carboxylic acid was activated by conversion to the NHS ester **11** with 2,5-dioxopyrrolidin-1-yl 2,2,2-trifluoroacetate (*N*-trifluoroacetoxy succinimide, TFA-NHS) that was prepared according to reference.^[52] Subsequently, 4-azido-*N*-(2-chloroethyl)butanamide (**12**) was obtained by amidation of **11** with 2-chloroethylamine hydrochloride. Cyclization of compound **12** in the presence of anhydrous K_2CO_3 led to the final product AzOxa (**13**) with an overall yield of 44% after the five synthesis steps.

2.1.4. Antifouling Motifs

The alkyne derivatives of the corresponding carboxy- and sulfobetaine were prepared by a ring opening reaction of pro-

piolactone for CB (**14**), and propan-1,3-sulton for SB (**15**), respectively with dimethylamino-2-propyne, according to the literature.^[53]

For synthesis of OEG (**16**, see **Scheme 1**), a threefold excess of triethylene glycol was deprotonated with sodium hydride and coupled to propargyl bromide. The monosubstituted product was separated from the reaction mixture by column chromatography on silica gel with an ethyl acetate/*n*-hexane mixture ($V/V = 3/1$) as eluent. For the synthesis of the oligoethylene glycol-sulfobetaine conjugate, the terminal hydroxy functionality of OEG was transformed into the tosylate **17** as effective leaving group by reaction with 4-toluenesulfonyl chloride. Subsequent substitution with dimethylamine lead to derivative **18** with a dimethyl amino group, which was subjected to the ring opening reaction with propan-1,3-sulton, resulting in the final product OEG-SB (**19**). The overall yield of 41% for this four-step synthesis route is attributed to the mediocre yield of 55% in first reaction step. Attempts to synthesize the analogous OEG-

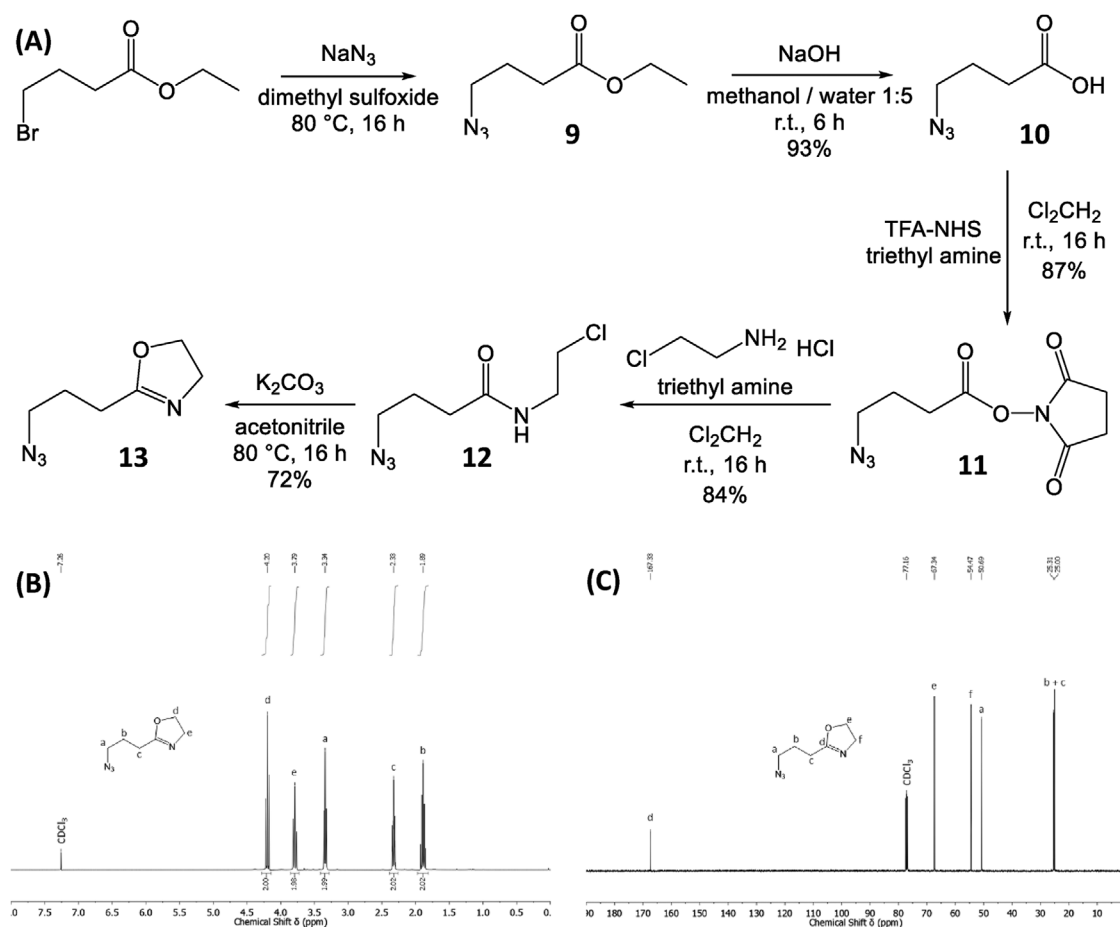
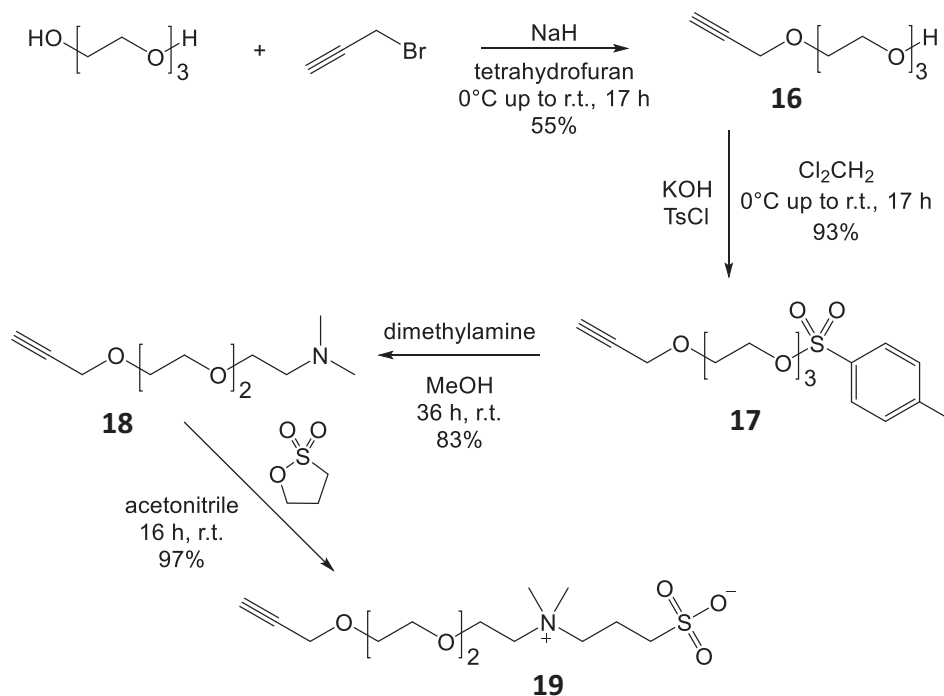


Figure 2. A) Synthesis of AzOxa (**13**) (TFA-NHS = 2,5-dioxopyrrolidin-1-yl 2,2,2-trifluoroacetate). B) ^1H -NMR spectrum of AzOxa (**13**) and C) ^{13}C -NMR spectrum of AzOxa (**13**), both measured at r.t. with 400 Hz in CDCl_3 .



Scheme 1. Synthesis of OEG (16) and OEG-SB (19).

CB with carboxy betaine end group at the OEG chain were not successful in our hands, for details see Chapter S17 (Supporting Information).

2.1.5. Two-Component Copolymers

Copolymers containing one or more types of main monomers as first component and the photocrosslinker monomer 4 as second component are defined here as two-component copolymers. The copolymerization behavior of photocrosslinker 4 was investigated in various ratios with the 2-alkyl-2-oxazoline main monomers EtOxa (6), iPrOxa (7), nPrOxa (8), and combinations thereof. Details for the resulting poly(2-oxazoline) copolymers, such as composition, molar mass, dispersity \bar{D} , and yield, are summarized in Table S1 (Supporting Information). The experimental data demonstrate good agreement between monomer feed and build-in ratio, and thus document the precise control over the polymer structures. The narrow molar mass distribution observed for almost all polymer systems indicate the quasi-living character of the performed polymerization reactions. Noteworthy, a general trend was observed for the series poly(EtOxa-co-BPOxa), with an increasing dispersity \bar{D} from 1.17 for poly(EtOxa) up to 1.55 for poly(EtOxa₉₀-co-BPOxa₁₀), which may be explained by the photocrosslinker monomer 4 apparently affecting the CROP mechanism by transfer or termination as potential side reactions. As expected, the glass points of the copolymers, as measured with modulated differential scanning calorimetry (M-DSC), vary systematically with the concentration of the BPOxa crosslinker units from 61.5 °C for pure poly(EtOxa) up to 66.5 °C for 100% poly(BPOxa), see Chapter S15 (Supporting Information).

2.1.6. Three-Component Copolymers

The three-component copolymers are defined by their composition, with the first component being the main monomer iPrOxa (7), the second component being the photocrosslinker monomer 4, and the third component being the azide-modified 2-oxazoline monomer 13 (AzOxa). The selection of the main monomer iPrOxa was based on previous measurements of the cloud points for binary copolymer solutions in water (see Figure S11, Supporting Information). In such experiments, the cloud point temperatures between 35–45 °C observed for the iPrOxa-AzOxa combination are quite suitable for applications involving proteins and living tissue. In contrast, a rather high temperature range of 60–75 °C was found for the combination of the monomers EtOxa and AzOxa, which is inconvenient in a biological context. Furthermore, previously performed temperature-dependent swelling experiments of photocrosslinked hydrogel films in water showed a well-defined, sharp volume transition at 32 °C for poly(iPrOxa-co-BPOxa). Such thermoresponsive behavior under physiological conditions can be exploited for actuation in active plasmonics and advanced biosensor devices.^[23–26]

Two photocrosslinkable iPrOxa-based poly(2-oxazoline)s with 6 and 10 mol% AzOxa (13), respectively, and 3 mol% benzophenone monomer 4 were synthesized using microwave-assisted CROP. Detailed information about the analysis of the three-component polymers is provided in the (Chapters S8,S9, Supporting Information) together with the data for the click-modified polymers discussed further below. Comparison of the iPrOxa homopolymer with the two-component polymers and the three-component polymers shows that both comonomers, the photocrosslinker 4 and the azide monomer 13, lead to broadening of the molar mass distribution.

2.1.7. Click-Modifications

The azide-containing three-component copolymers were modified with the alkyne-functionalized antifouling motifs **14**, **15**, **16**, and **19** via copper(I)-catalyzed azide-alkyne cycloaddition (CuAAC), see **Figure 3A**. Furthermore, the commercially available 4-pentynoic acid (COOH, **20**) was also conjugated to the azide-based polymer by this coupling reaction to introduce free carboxylic acid functions into the polyoxazoline backbone, which also allows further functionalization, for example, with bioligands like antibodies. The progress of the CuAAC reaction was monitored by IR spectroscopy, following the azide absorption band located at $\approx 2100\text{ cm}^{-1}$, which indicated complete conversion of the azide functionality. The CuAAC-modified polymers were dialyzed against water to remove copper sulfate, sodium ascorbate, and any excess of the respective alkynes.

The data from the SEC measurements indicated striking differences between the azide-containing parent polymer and the click-modified systems with pending antifouling motifs, even though the degree of polymerization does not change during the CuAAC click modification (apparent molar mass and dispersity data are presented in **Figure 3D,E**, the original GPC data are provided in Chapter S18, Supporting Information). For the parent system poly(iPrOxa₉₁-co-BPOxa₃-co-AzOxa₆) with 6 mol% azide functions, an average molar mass of $27.7 \times 10^3\text{ g mol}^{-1}$ was determined, which corresponds very well to the expected values of $30\text{--}35 \times 10^3\text{ g mol}^{-1}$ for the monomer-initiator ratio of $\approx 300/1$ used in the CROP synthesis of this polymer. Notably, the polymers with the antifouling motifs in the side chains showed a trend to higher apparent molar masses and a considerable increase of their dispersities. Based on the masses of the alkyne fragments, the order of the polymer mass increase is expected to follow the side chain modification with $\text{N}_3 < \text{COOH} < \text{CB} < \text{OEG} < \text{SB} < \text{OEG-SB}$, resulting in an approximate maximum mass increase of 10% for **OEG-SB**. In contrast, the apparent molar mass as measured by SEC follows the unexpected order of the polymer functionality $\text{N}_3 < \text{COOH} < \text{OEG} < \text{OEG-SB} < \text{SB} < \text{CB}$ with almost 30% apparent mass increase for **CB**. This might be explained as follows. In SEC analysis, the relative molar mass is deduced from the hydrodynamic radius of the polymer coil in relation to a calibration standard. Thus, the apparent increase of the molar mass in the CuAAC-modified polymers is based on the increase of their hydrodynamic radius. Such coil expansion is caused by the addition of the antifouling side chains with zwitterionic character, which results in polar and solvation effects that influence coil swelling and consequently result in ill-defined molar mass values.

Surprisingly, for the 10 mol% azide-functionalized base polymer poly(iPrOxa₈₇-co-BPOxa₃-co-AzOxa₁₀), the trend of the apparent molar mass variation is in stark contrast to the 6 mol% polymers above, showing the opposite behavior. Here, a significant decrease of the apparent molar mass was observed, diminishing from $28.3 \times 10^3\text{ g mol}^{-1}$ for the parent polymer poly(iPrOxa₈₇-BPOxa₃-AzOxa₁₀), following the order $\text{N}_3 > \text{OEG} > \text{OEG-SB} > \text{SB} > \text{CB}$, to $9.5 \times 10^3\text{ g mol}^{-1}$ for poly(iPrOxa₈₇-co-BPOxa₃-co-CB₁₀). This reversed trend may be caused by the increased number of charges on the backbone, which potentially leads to an aggregation of single polymer chains (coil to globule transi-

tion) and therefore a decrease in hydrodynamic radius and apparent average molar mass in SEC. This hypothesis is further corroborated by the opposing thermal response of poly(2-alkyl-2-oxazoline)s and polybetaines, reported in the literature.^[54–56] Poly(2-alkyl-2-oxazoline)s can show a LCST behavior in aqueous media, for which an increase in the overall polarity leads to an improved water solubility and consequently an increase in the cloud point temperature. Yet, several polybetaine systems are known to possess an upper critical solution temperature (UCST) in water, which is based on the attractive interaction between the zwitterionic groups and exactly opposite to the LCST behavior of the poly(2-alkyl-2-oxazoline)s. In the case of the present polymer samples based on poly(iPrOxa₉₁-co-BPOxa₃-co-AzOxa₆) with a lower degree of modification of 6 mol%, the coupling of the antifouling motifs indeed increases the solubilization with water, leading to coil expansion, as observed by the apparent molar mass values from SEC, and an increased cloud point (see **Figure 4**). For the higher degree of modification with 10 mol% antifouling motifs, such competing UCST character by attractive zwitterion interaction in the side chains may become dominant over the polarity of the polyoxazoline backbone, which leads to a compaction of the polymer chains with the reduced hydrodynamic radius and consequently a lower apparent mass value in dimethylacetamide used as solvent in SEC. Yet, the overall hydrophilicity of the polymer seems to be further increased as reflected in a still higher cloud point compared to the 6 mol% samples (see **Figure 4**).

2.1.8. Anchor Molecule

For attaching the polymers to a gold substrate by photoactivation, the gold anchor molecule with benzophenone groups BPdiS (**22**) was synthesized as previously reported.^[25] Briefly, 3,3'-dithiodipropionic acid was converted into an active ester with NHS and TFAA in the first step. In the second step, a nucleophilic substitution of the active ester with (4-(aminomethyl)phenyl)(phenyl)methanone yielded the target molecule BPdiS (**22**) in an overall yield of $\approx 41\%$.

2.2. Thermal Properties of Aqueous Poly(2-oxazoline) Solutions

As the synthesized polymers are targeted for advanced biosensor applications, their behavior in aqueous environments needs to be understood. In this respect, we have studied the temperature-dependent solution behavior of two- and three-component copolymers in water by turbidimetry with a UV/VIS spectrometer and compared it to that of the respective poly(2-alkyl-2-oxazoline) homopolymers. All measurements were performed using 0.3 wt.% aqueous polymer solutions with a heating and cooling rate of 1 K min^{-1} , while recording the transmittance at a wavelength of 550 nm. The cloud point was defined as the temperature, at which a transmittance of 50% was reached.

Figure 5C shows the dramatic decrease of the cloud points from about $70\text{ }^\circ\text{C}$ to $20\text{ }^\circ\text{C}$ with increasing BPOxa content of up to 6 mol% for poly(EtOxa-co-BPOxa), and for poly(iPrOxa-co-BPOxa) a cloud point reduction from $\approx 40\text{ }^\circ\text{C}$ to $\approx 20\text{ }^\circ\text{C}$. The drop of the cloud points with increasing BPOxa content can be attributed to the less hydrated benzophenone groups compared

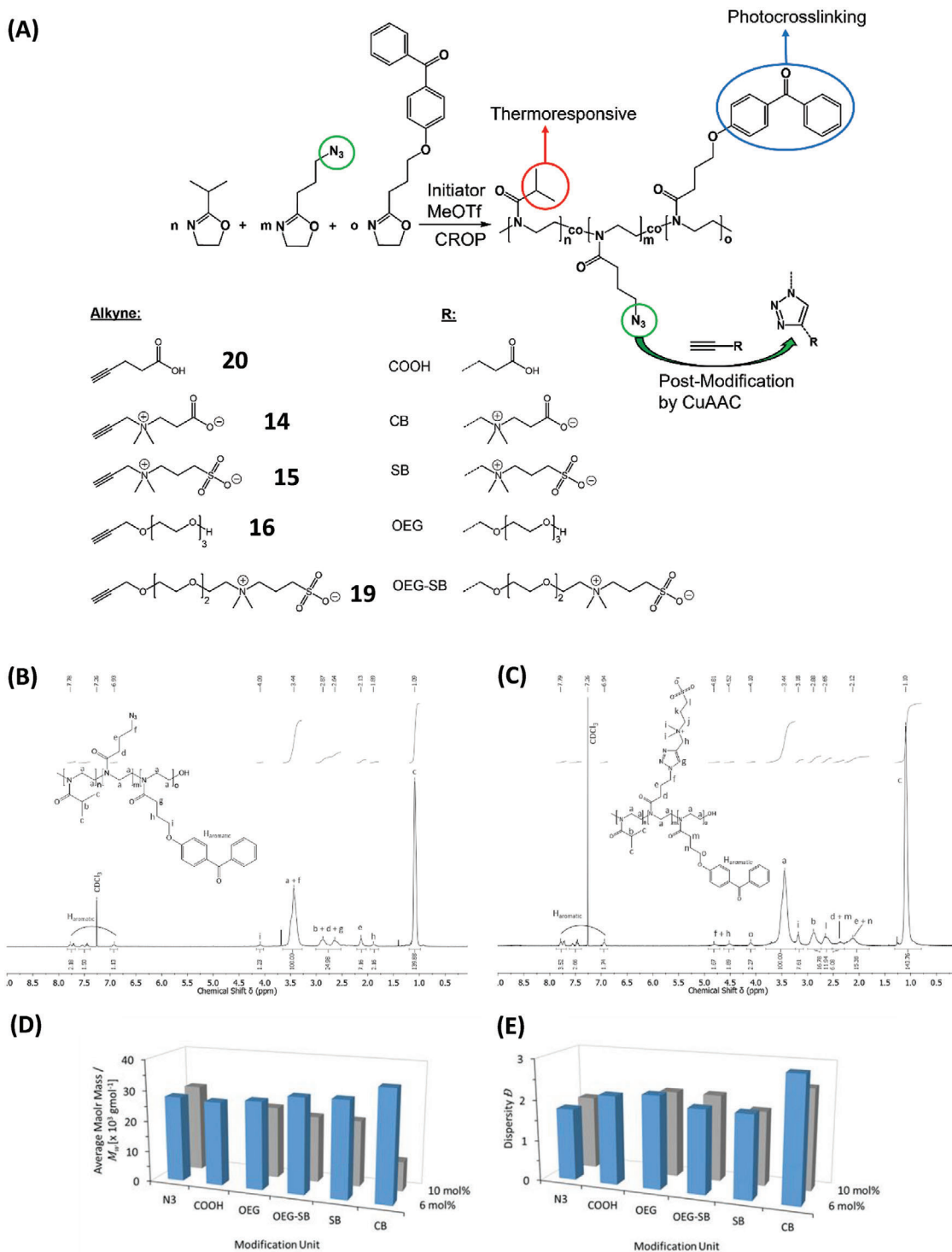
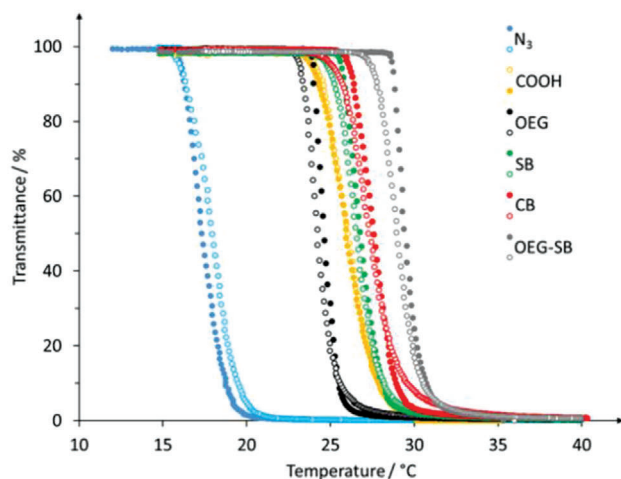
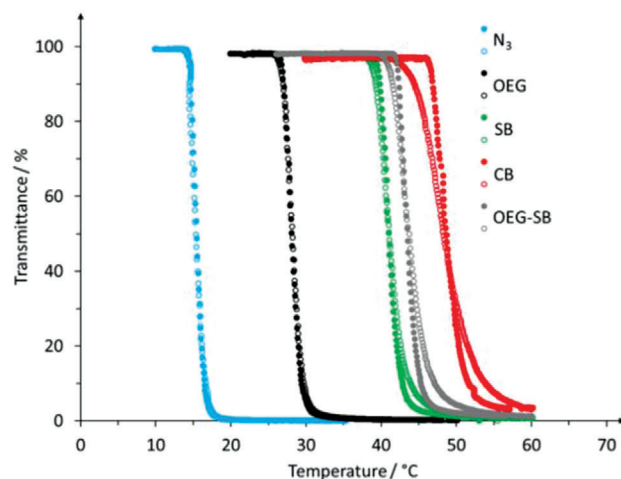


Figure 3. A) Synthesis and CuAAC click modification of the three-component copolymers containing iPrOxa (7) as main monomer, AzOxa (13) as modification side, and BPOxa (4) for photocrosslinking. B) $^1\text{H-NMR}$ spectrum of poly(iPrOxa₈₇-BPOxa₃-AzOxa₁₀) in CDCl_3 before CuAAC click coupling. C) $^1\text{H-NMR}$ spectrum of poly(iPrOxa₈₇-BPOxa₃-SB₁₀) in CDCl_3 after modification of AzOxa with SB. D) Apparent molar mass average and E) dispersity in dependence of the modification unit after CuAAC click coupling for the different antifouling motifs.

(A) 6 mol% antifouling motifs



(B) 10 mol% antifouling motifs



(C)

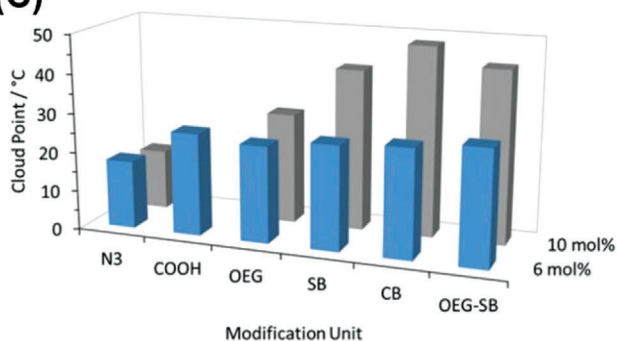


Figure 4. Cloud point dependence on type of functional group for 0.3 wt.% aqueous solutions of the poly(iPrOxa-co-BPOxa-co-AzOxa) systems, as determined by UV/VIS turbidity measurements at a wavelength of 650 nm and a heating rate of 1 K min⁻¹. A) Transmittance curves of non-modified and modified poly(iPrOxa₉₁-co-BPOxa₃-co-AzOxa₆) and B) poly(iPrOxa₈₇-co-BPOxa₃-co-AzOxa₁₀). C) Cloud point comparison between non-modified and modified poly(iPrOxa₉₁-co-BPOxa₃-co-AzOxa₆) and poly(iPrOxa₈₇-co-BPOxa₃-co-AzOxa₁₀).

to the more polar 2-ethyl and 2-isopropyl amide side chains. The transmittance curves in Figure 5A,B are characterized by sharp transitions for both, the heating and cooling cycles, demonstrating reversible LCST-type switching from a hydrophilic state below the cloud point temperature to a more hydrophobic state beyond this point. A hysteresis as narrow as 0.5 K was observed for the majority of the investigated polymers. Due to the insolubility of the copolymer poly(nPrOxa₉₄-co-BPOxa₆) in water, a comparison of the cloud point with the corresponding homopolymer poly(nPrOxa) could not be performed. Since the temperature range of the cloud points for poly(iPrOxa-co-BPOxa) between ≈20 °C and ≈40 °C is most appropriate for the anticipated biosensor applications, the cloud point measurements for the three-component polymers discussed below were only performed with the iPrOxa system.

After modification of the parent polymers poly(iPrOxa-co-BPOxa-co-AzOxa) containing 6% or 10% azide groups (abbreviated as N3 in Figure 4) by CuAAC click coupling with the alkyne motifs COOH (20), CB (14), OEG (15), SB (16), and OEG-SB (19), their cloud points in aqueous solutions were determined

by turbidity measurements, as above. The experiments were performed with 0.3 wt.% aqueous polymer solutions and a heating rate of 1 K min⁻¹, recording the transmittance at a wavelength of 650 nm. Again, heating and cooling cycles were performed for each polymer solution and the cloud point was defined as the temperature, at which the transmittance dropped to 50%. A significant increase of the cloud point temperature was observed for all polymers after modification with the antifouling motif, as depicted in Figure 4. For the polymers with 6 mol% coupling sites, all types of modification showed a clear increase of the cloud point by ≈5–10 K starting from 18 °C for the 6 mol% azide-containing polymer. For the polymers with 10 mol% coupling sites, the cloud point increase was even more pronounced, specifically for the zwitterionic systems SB, CB, and OEG-SB, reaching almost 50 °C compared to 15 °C for the 10 mol% azide-containing polymer. All polymers could be reversibly switched from a hydrophilic to a hydrophobic state with a minor hysteresis between the heating and cooling cycle of ≈0.5 to 1 K. The plausible explanation for the observed cloud point increase in all alkyne-modified samples is a much stronger

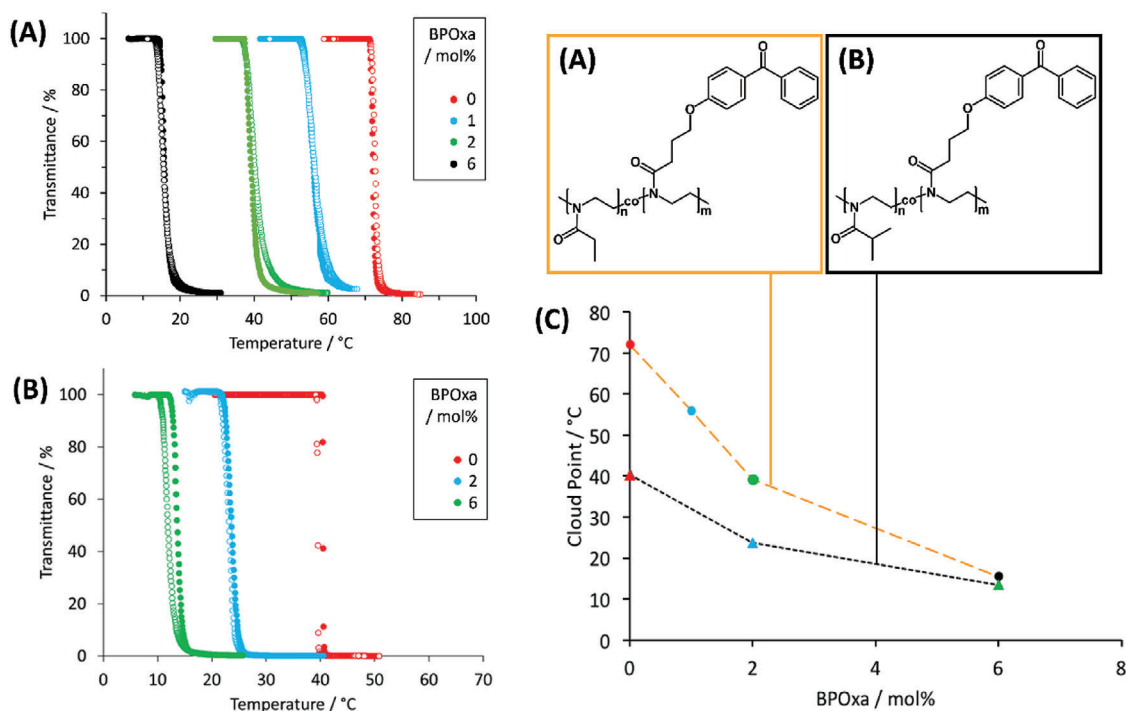


Figure 5. Transmittance curves at 550 nm for aqueous solutions of A) poly(EtOxa-co-BPOxa) and B) poly(iPrOxa-co-BPOxa) with polymer concentrations of 3 mg ml⁻¹, recorded with a heating and cooling rate of 1 K min⁻¹ (filled circles indicate heating and open circles cooling). C) Cloud point dependence on benzophenone content for poly(EtOxa-co-BPOxa) and poly(iPrOxa-co-BPOxa). Color codes in (C) correspond to BPOxa content in polymer samples of (A) and (B), respectively. Cloud point error: ±1 K.

hydration of the highly polar side chains, which results in a higher enthalpy of mixing ΔH_M compared to the non-modified parent polymer poly(iPrOxa-co-BPOxa-co-AzOxa).

2.3. Photocrosslinking and Thermal Properties of Poly(2-oxazoline) Networks

To investigate the temperature-dependent swelling of surface attached hydrogel films by SPR/OWS, the benzophenone-containing poly(2-alkyl-2-oxazoline) systems, comprising two- and three-component polymers, were photocrosslinked by irradiation with UV light. For the covalent attachment of such hydrogel layers during photocrosslinking, the SPR/OWS substrates were modified as follows. First, Au substrates were immersed into 1 mM solutions of BPdIS (22) in dimethyl sulfoxide and then rinsed with dimethyl sulfoxide and ethanol, followed by drying under a stream of nitrogen. Onto these BPdIS-coated substrate, the benzophenone-containing polymers were spin coated at 2000 rpm from a 6–10 wt.% ethanolic solution, resulting in layer thicknesses of 350–850 nm after drying. The dry polymer layers were irradiated with UV light of 365 nm an irradiation dose of 8 J cm⁻² (for two-component copolymers) and 12 J cm⁻² (for three-component copolymers) under exclusion of oxygen, to induce simultaneous crosslinking and covalent attachment to the substrate. The crosslinked samples were inserted into an electrically heatable SPR sample holder, in which the polymer network layers were swollen and rinsed with water for 60 min to ensure removal of residual soluble components in the hydrogel

film. Initial reflectivity curve was recorded at room temperature and then, after each increasing temperature step, the layers were equilibrated for 15 min. The swelling properties were analyzed at each temperature step by SPR/OWS upon resonant excitation with attenuated total reflection in Kretschmann configuration. Under SPR/OWS conditions, surface plasmons and dielectric waveguide-guided waves are phase-matched with the excitation light beam to probe the polymer network films. This optical coupling is manifested as a series of narrow dips at distinct angles in the angular reflectivity spectra $R(\theta)$, see Figure S13 (Supporting Information). The refractive indices n and thicknesses d of the polymer films were determined from the angular reflectivity spectra $R(\theta)$ either in the dry (n_{dry} , d_{dry}) or swollen ($n_{swollen}$, $d_{swollen}$) state. As these measurements were performed in situ, the changes in thickness and refractive index could be tracked in real time upon variations of temperature or solvent. The swelling ratio SR and surface mass density Γ were calculated from the refractive indices and layer thicknesses according to Equations (2) and (3), see experimental part for more details.

Figure 6 depicts the temperature-dependent swelling ratios, which are the inverse of the polymeric volume fractions Φ , for the water-swollen hydrogels composed of different poly(2-alkyl-2-oxazoline) networks. The swelling ratios of these hydrogel layers at 20 °C follow the order of their cloud points in aqueous solution (T_{CP}), indicated above the chemical structures of each copolymer. Yet, the estimated center temperatures of the volume transitions for the polymer networks, at which the gel is half collapsed, lie significantly higher than the T_{CP} of the respective polymer solutions. Here, the center temperature is defined in analogy to

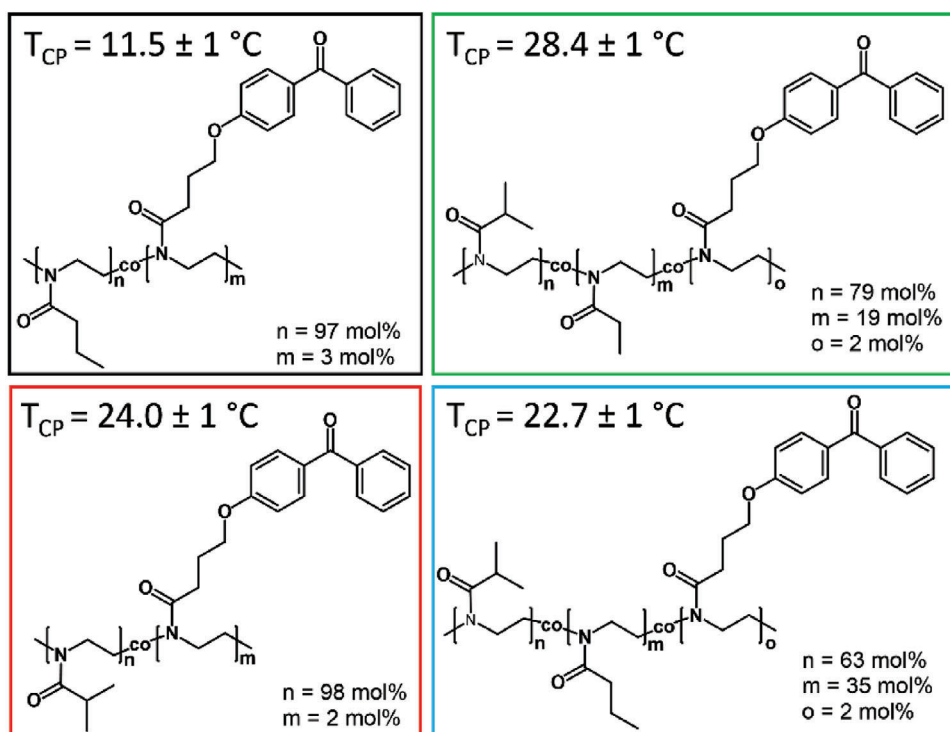
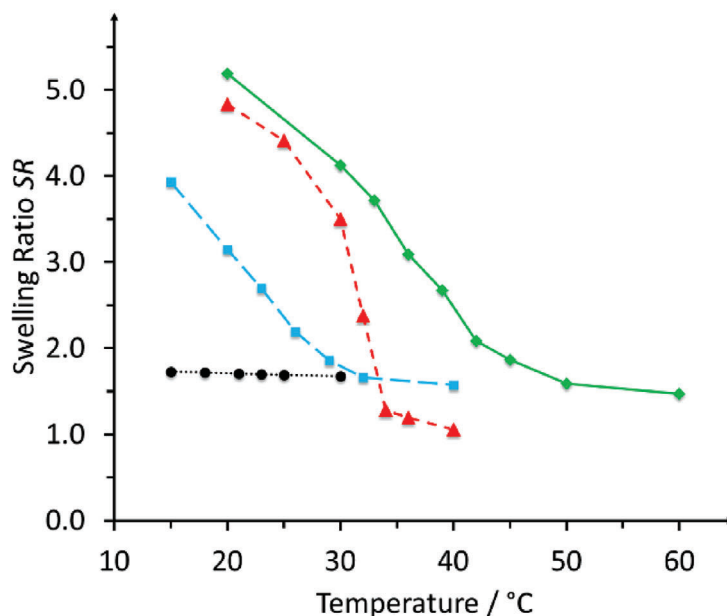


Figure 6. SPR/OWS measurements of the temperature-dependent swelling ratio in water for surface-attached hydrogel layers based on four different benzophenone-containing poly(2-alkyl-2-oxazoline)s.

the cloud point temperature, at which a transmittance of 50% is reached, and is estimated on the basis of the experimentally accessible temperature range. The shift of the transition temperature can be explained with the change in the polymer volume fraction from $\Phi \approx 0.03$ for the polymer solutions to $\Phi > 0.6$ in the hydrogels.

This trend follows the theoretical prediction of the phase transition curves, for which the branch on the right side of the LCST minimum increases with increasing polymer volume fractions and skews toward smaller volume fractions with increasing chain lengths.^[57] This behavior is further illustrated for a range of varying volume fractions in the polymer solutions

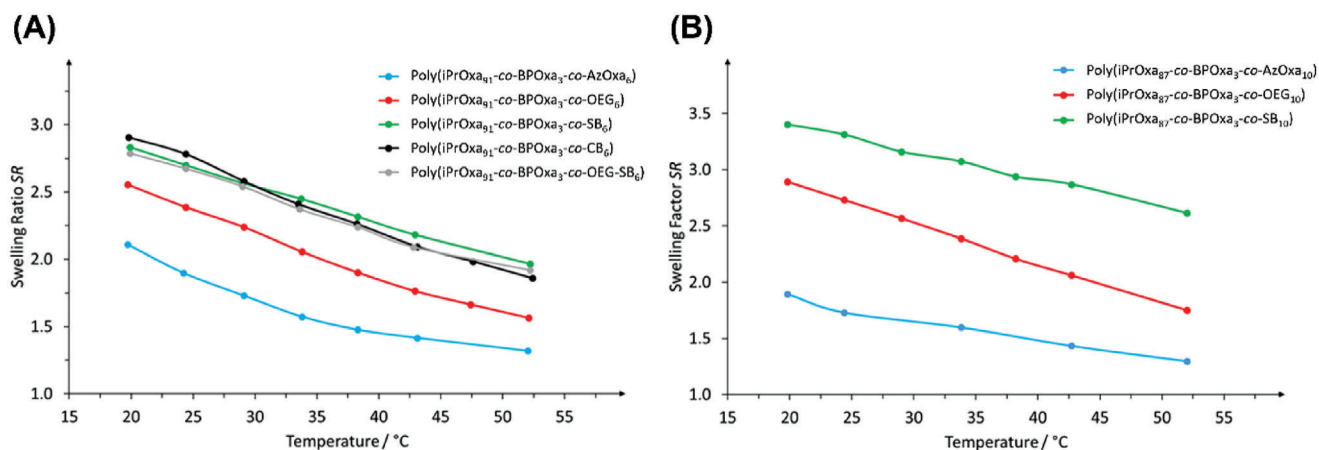


Figure 7. Temperature-dependent swelling of hydrogel films made from CuAAC-modified poly(2-alkyl-2-oxazolines) with A) 6 mol% and B) 10 mol% antifouling motifs in comparison to the non-modified AzOxa systems (blue), as determined by OWS.

in Figure S10 (Supporting Information). For all investigated polymer systems, a substantial sigmoidal drop in the swelling ratio was observed with increasing temperature, except for poly(*n*PrOxa₉₇-*co*-BPOxa₃), in which the volume transition lies below the limiting minimum temperature of 15 °C accessible by the SPR equipment. These experiments confirm that the surface-attached poly(2-alkyl-2-oxazoline) hydrogel layers can be reversibly switched between a swollen and collapsed state by temperature variation around the volume phase transition (see Figure S14, Supporting Information). Simultaneously, the Young's modulus switches between a soft swollen network at low temperatures and a more rigid collapsed film above the volume phase transition, as observed by atomic force microscopy indentation measurements (see Figure S22, Supporting Information, red circles). An additional variation of the Young's modulus can be achieved via a different crosslinking density effected by modulation of the irradiation dose (see Figure S22, Supporting Information, green circles). A sharp volume transition was observed in the interval of ≈ 5 K for the two-component system poly(*i*PrOxa₉₈-*co*-BPOxa₂), which contains a single main monomer (*i*PrOxa) that is responsible for the LCST behavior. In contrast, the phase transition region is significantly widened to several $\times 10$ K for the two-component systems poly(*i*PrOxa₆₃-*co*-*n*PrOxa₃₅-*co*-BPOxa₂) and poly(*i*PrOxa₇₉-*co*-EtOxa₁₉-*co*-BPOxa₂) with a mixture of two LCST-inducing main comonomers (*i*PrOxa and *n*PrOxa, *i*PrOxa and EtOxa). Noteworthy, further broadening of the phase transition region was found for the surface-attached hydrogel layers with the three-component systems including the azide or antifouling motifs, as shown in Figure 7A.

Due to the high polarity of the zwitterionic side chains, the three-component polymer systems were irradiated with UV light dose of 12 J cm^{-2} (compared to 8 J cm^{-2} for the two-component samples), to ensure stable layer formation and prevent hydrogel layer delamination. The results depicted in Figure 7 show a significant increase of the swelling ratio upon introduction of the antifouling motifs by CuAAC modification, with the highest swelling ratios observed for the zwitterionic systems. Following the order of their cloud points in aqueous solution (Figure 4), which can be seen as an indicator for the polarity of the polymers, the swelling ratios of the OEG-modified polymers lie between the

least polar parent azide polymers and the modified systems bearing highly polar zwitterionic groups. The increase of the swelling ratio is more pronounced for the polymers with a higher content of the respective modification motif (10 mol% vs 6 mol%), again following the trend of the cloud points in water shown above. All systems are characterized by a gradual decrease of the swelling ratio with increasing temperature over the range of 20–52 °C. The residual water content of the collapsed systems at the maximum temperature was found to be highest for the zwitterionic polymer systems. As above for the two-component copolymer systems, repeated heating and cooling cycles of the three-component samples demonstrated full reversibility of the swelling behavior.

2.4. Antifouling Properties of Modified Poly(2-oxazoline) Networks

HBP represents an important biological fluid, which is used in numerous bioanalytical techniques (e.g. detection of specific biomarkers of diseases) or therapy (for example, apheresis and dialysis). PBS is a frequently used medium in blood-related research, as it exhibits pH of 7.4 and contains key ions at concentration close to physiological conditions. To investigate the suitability of the three-component hydrogels as antifouling coatings in contact with HBP, polymer network layers were prepared on BPdis-modified gold surfaces by photocrosslinking, analogous to the SPR/OWS swelling experiments above. The three-component hydrogels were based on poly(*i*PrOxa₈₇-*co*-BPOxa₃-*co*-AzOxa₁₀), which was modified with 10 mol% of the antifouling motifs CB (14), SB (15), OEG (16), and OEG-SB (19), respectively. The swelling properties of these hydrogel films were first examined in PBS and afterward their changes occurring in contact with pooled HBP were assessed at room temperature (25 °C).

The reference hydrogel film from poly(*i*PrOxa₈₇-*co*-BPOxa₃-*co*-AzOxa₁₀) with unreacted azide groups (N_3), crosslinked with 5 J cm^{-2} , exhibited the lowest swelling ratio of $SR_{\text{PBS}} \approx 1.6$ in PBS (shown in Figure 8) compared to $SR_{\text{H}_2\text{O}} \approx 1.7$ in water. The reduced swelling in PBS buffer compared to pure water for the uncharged polymer hints to a reduction of the solvent quality owing to the presence of ions. Introduction of OEG

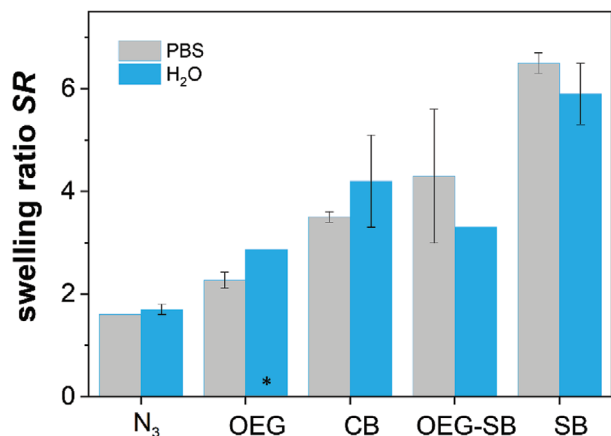


Figure 8. Swelling ratios (SRs) of poly(2-alkyl-2-oxazoline) hydrogel films with 10 mol% antifouling motifs, crosslinked with 5 J cm^{-2} (* 12 J cm^{-2}) at the wavelength of 365 nm, and swollen in PBS (10 mM, pH 7.4) in grey and in water, blue. Error bars were derived from standard deviation of triplicates.

groups into the three-component copolymer led to a minor increase of the swelling ratio to $SR_{\text{PBS}} \approx 2.3$ in PBS, which is attributed to an enhanced hydrophilicity of the polymer system through the OEG side chains. Yet, in water the swelling ratio for this system is higher despite the increased degree of crosslinking ($SR_{\text{H}_2\text{O}} \approx 2.8$ at 25°C , 12 J cm^{-2}), again indicating a decrease in solvent quality for PBS. Even higher swelling ratios were observed for the hydrogel films comprising the zwitterionic CB groups with $SR_{\text{PBS}} \approx 3.5$ ($SR_{\text{H}_2\text{O}} \approx 4.2$) and OEG-SB moieties with $SR_{\text{PBS}} \approx 4.3$ ($SR_{\text{H}_2\text{O}} \approx 3.3$), respectively, while the most prominent effect was present in the SB system with the highest swelling ratio of $SR_{\text{PBS}} \approx 6.5$ ($SR_{\text{H}_2\text{O}} \approx 5.9$). The substantial increase in swelling of the SB system can be explained by the increased degree of ionization resulting from the lower pK_a value of the corresponding sulfonic acid group (pK_a typically below 1) compared to the carboxylic acid (pK_a typically ≈ 5) related to the CB moiety.^[58,59] This more pronounced ionization in the SB system promotes stronger solvation and consequently enhanced swelling.^[60,61] Interestingly, the combination of the hydrophilic OEG chain with the highly polar SB motif for OEG-SB does not substantially increase the swelling ratio compared to the single CB functionalization, but rather leads to an intermediate swelling ratio in PBS. As OEG side chains are known to introduce a LCST behavior, a competing influence between OEG and SB (inherent UCST characteristics) might be responsible here. A further notable effect is the inversion of the swelling trend in pure water, for which the values of N₃, OEG, and CB lie above the values in PBS, while for OEG-SB and SB the PBS values are higher. Apparently, the strong charge screening of the SB moieties in PBS prevents their electrostatic aggregation, which is accompanied by a stronger swelling. As investigated above for pure water (Figure 7), the hydrogel layers can be reversibly collapsed also in PBS buffer, shown in Figure S24 (Supporting Information).

After this initial assessment of the hydrogels in contact with PBS buffer, the effect of HBP on the swelling ratio SR and surface mass density Γ was investigated to evaluate their applicability as antifouling coatings. For this purpose, the films were

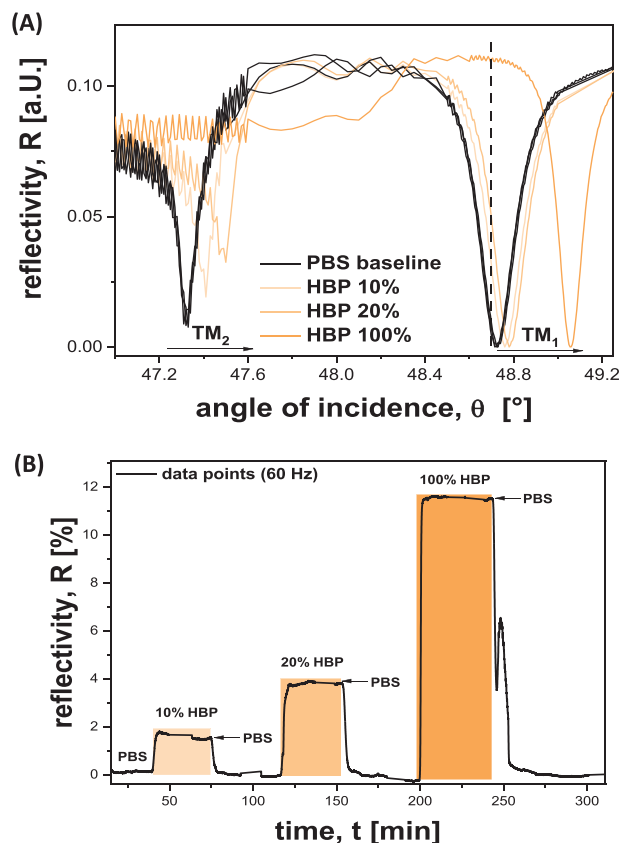


Figure 9. Examples of OWS measurements indicating the changes in reflectivity for poly(2-alkyl-2-oxazoline)-based hydrogel with SB moieties. A) Normalized reflectivity spectra $R(\theta)$ measured upon incubation with HBP diluted to 10 and 20% and with undiluted HBP. B) Respective kinetics of reflectivity changes measured over time at fixed angle $\theta = 48.7^\circ$ (after baseline correction due to a drift in the signal). Colored sections indicate the contact time intervals with different dilutions of HBP.

first swollen in PBS to reach an equilibrium and to establish a baseline for the reflectivity value $R(\theta)$ at a fixed angle of 48.7° . This angle was positioned at the sharp slope of the resonance dip associated with the excitation of the TM_1 mode (see example in Figure 9A) to assess the effect of HBP in the kinetics mode of the SPR/OWS set-up. In this kinetics mode, the variation in reflectivity $R(\theta = 48.7^\circ)$ was monitored upon changing the medium from PBS to whole HBP and HBP diluted to 10 and 20% with PBS with an incubation time of 15 min. The kinetics for the poly(2-alkyl-2-oxazoline)-SB polymer network in Figure 9B reveal an increase in the reflectivity upon incubation with HBP medium, and a drop reversing back to the original baseline upon subsequent rinsing with PBS. These observations indicate a complete release of all HBP components from the poly(2-alkyl-2-oxazoline)-based polymer networks after washing with PBS, with no irreversible attachment of HBP compounds being visible. All investigated poly(2-alkyl-2-oxazoline)-based hydrogel films showed the same qualitative behavior, suggesting that all systems perform as efficient protein-repellent antifouling coatings.

In order to determine changes occurring directly in contact with HBP, respective reflectivity scans $R(\theta)$ were measured and

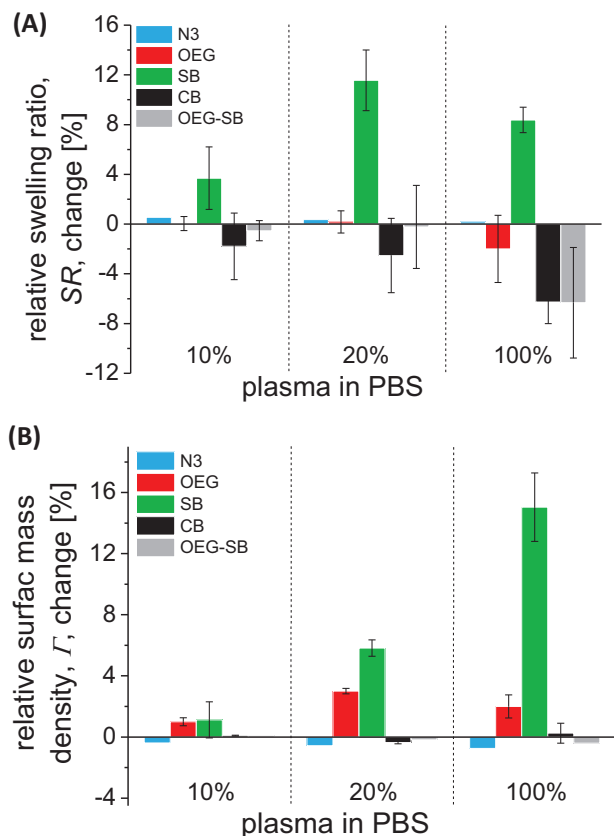


Figure 10. A) Relative swelling ratio change at different concentrations of HBP for hydrogel films with different side-chain motifs. Error bars indicate standard deviation from triplicates. Data fitted with asymptotic fit. Relative values calculated in respect to data for pure PBS (0% HBP). B) Relative surface mass density change at different concentrations of HBP for the same polymers as in (A).

by simultaneous probing with TM_1 and TE_0 modes the associated optical properties were determined. Angular reflectivity scans presented in Figure 9A show a shift of the TM_1 and TM_2 resonances to higher angles when contacted to HBP, reverting to the original positions after rinsing with PBS, in accordance with the kinetics data above. Bulk refractive index HBP sample was first determined as of $n_{\text{solvent}} = 1.3340, 1.3342, 1.3350, 1.3445$ for 0, 10, 20, 100% HBP, respectively, from the critical angle position.

Then, variations in thickness d_{swollen} and refractive index n_{swollen} of the hydrogel layer were evaluated to follow changes in swelling ratio SR and surface mass density Γ , as summarized in Figure 10. The polymer networks carrying N3 and OEG motifs show no change in the SR and surface mass density Γ when contacted with HBP. Contrary to these samples, hydrogel films carrying OEG-SB and CB moieties behave differently as their SR decreased by $\approx 6\%$ in pure HBP. Interestingly, an opposite effect was measured for the polymer networks with SB, for which SR increased by more than 7% in presence of whole HBP. All hydrogel films show no measurable change in surface mass density Γ when contacted with HBP, except the film made from the polymer bearing SB groups. The data suggest that only a minute amount of biomolecules was able to diffuse into the polymer network with N3, OEG, CB, and OEG-SB motifs. Ap-

parently, the measured increase in surface mass density of $\Delta\Gamma = 28 \pm 15 \text{ ng mm}^{-2}$ indicates that the hydrogel film with SB groups possesses a sufficiently open structure, through which HBP constituents can reversibly diffuse. These observations are particularly interesting, as the ability to reversibly uptake and release components from HBP is of high importance for applications in biosensing with such hydrogel films as binding matrices.

3. Conclusion

The present study demonstrates a remarkable performance of hydrogel coatings against fouling by undiluted human blood plasma, exploiting surface-attached, water-swollen polymer networks from photocrosslinkable poly(2-alkyl-2-oxazoline)s with pendent betaine moieties. The developed synthesis route, which allows full control over the polymer composition, employs a monomer toolbox comprising the novel benzophenone oxazoline BPOxa for photocrosslinking and the azide-functionalized oxazoline AzOxa for click-coupling of alkyne-modified antifouling motifs from the class of carboxy- and sulfobetaines. This approach provides access to a modular architecture with 2-alkyl-2-oxazolines as backbone-forming main monomers, which, depending on the substitution pattern, can entail an LCST-type thermoresponsiveness to reversibly vary the hydrogel film thickness with temperature. The analysis of the thermal response revealed a striking increase of several Kelvin for the volume transitions of water-swollen crosslinked networks in comparison to the cloud points of the polymers in solution, resulting from the higher polymer volume fraction in the networks with $\Phi > 0.6$ compared to the solutions with $\Phi \approx 0.03$. The SPR/OWS investigation of the hydrogel coatings in contact with human blood plasma shows specifically for the sulfobetaine-functionalized system an efficient penetration of the swollen polymer network by the plasma components, yet a complete release of all components upon rinsing with aqueous buffer, rendering this material as a versatile protein-repellant coating and promising matrix for advanced biosensor architectures.

4. Experimental Section

Synthesis Procedures: The syntheses routes for all monomers, polymers, antifouling motifs, and click-modified polymers as well as a list of the used materials and instrumentation can be found in the Supporting Information.

Turbidimetry Measurements: The temperature-dependent solution behavior of the polymers in water was determined by turbidimetry with UV/VIS spectroscopy. All measurements were performed using 0.3 wt.% aqueous polymer solutions with a heating and cooling rate of 1 K min^{-1} , while recording the transmittance at a wavelength of 550 or 650 nm. The cloud point was defined as the temperature, at which a transmittance of 50% was reached.

Preparation of Surface Attached Hydrogel Films: BK7 glass slides were coated with chromium (2 nm) and gold (50–55 nm) by vacuum thermal evaporation (HHV Auto 306 from HHV LTD). These substrates were directly immersed for 16 h into a 1 mm solution of 3,3'-disulfanediylbis[N-(4-benzoylbenzyl)propanamide] (BPdS, **22**) dissolved in dimethyl sulfoxide in order to form a SAM. The samples were rinsed with ethanol and dried by a steam of nitrogen. Ethanolic solutions of the oxazoline-based polymers (6–10 wt.%) were deposited by spin coating (2000 rpm for 120 s) onto the BPdS-modified gold substrates. The obtained polymer layers were dried for 4 h at 50 or 80 °C in a vacuum oven. The dry polymer layers

were crosslinked under argon atmosphere with UV light at wavelength of $\lambda = 365$ nm with irradiation doses between 4 and 20 J cm⁻².

SPR/OWS Analysis of Swollen Thin Hydrogel Films: The crosslinked polymer layers attached to the BPdIS-modified gold substrates were characterized in the dry and swollen state by surface plasmon resonance combined with optical waveguide spectroscopy (SPR/OWS). The optical system utilized attenuated total reflection in Kretschmann configuration as previously reported.^[44] Briefly, a polarized He-Ne laser ($\lambda = 632.8$ nm) was sent through a high refractive index prism composed of LASFN9 glass, to which a glass substrate with a thin metal layer and anchored hydrogel film was optically matched by a high refractive index oil. A flow-cell with a volume of 25 μ L was clamped against the glass substrate. This assembly was mounted on a rotation stage in order to measure changes in the reflected laser beam intensity as a function of the angle of incidence $R(\theta)$ by a photodiode connected to a lock-in amplifier (EG&G, Model 5210). The flow-cell was temperature-controlled by a Peltier element via a dedicated driver (LF13751, Wavelength Electronics, USA). Tygon LMT-55 tubings (Ismatec, Germany) with an inner diameter of 0.25 or 0.62 mm were used with a peristaltic pump (Ismatec, Germany) to transport liquid samples over the sensor surface. The measured angular reflectivity scans $R(\theta)$ were fitted by a Fresnel reflectivity model with the software WinSpall (Max Planck Institute for Polymer Research, Mainz, Germany). By fitting multiple resonant features associated with the excitation of TE₀, TM₁ and TM₂ modes allowed the determination of the thickness d_{dry} and the refractive index n_{dry} of the polymer networks in the dry state (in contact with air) and the thickness d_{swollen} and the refractive index n_{swollen} of the swollen polymer networks (in contact with a liquid). Birefringence was omitted and thus all refractive indices were assumed to be identical for TM and TE polarizations. The optical parameters of all other materials below the polymer layers (Cr, Au, linkers) were determined by reference samples without polymer layers. The polymer volume fraction of the film in the swollen state was calculated by the effective medium theory from the measured refractive indices in the dry and swollen states, according to Equation (1).^[45]

$$\Phi = \frac{n_{\text{swollen}}^2 - n_{\text{solvent}}^2}{n_{\text{swollen}}^2 + 2n_{\text{solvent}}^2} / \frac{n_{\text{dry}}^2 - n_{\text{solvent}}^2}{n_{\text{dry}}^2 + 2n_{\text{solvent}}^2} \quad (1)$$

Here, n_{solvent} is the refractive index of solvent (water, PBS, or HBP).

The swelling ratio of the film was determined from the measured thicknesses in the dry state d_{dry} and in contact with aqueous media d_{swollen} following Equation (2).

$$SR = d_{\text{swollen}}/d_{\text{dry}} \quad (2)$$

Pooled HBP was obtained from Innovative Research (USA). Diffusion of biomolecules from HBP into the polymer network results in changes of the hydrogel swelling state and was expressed as variation in the surface mass density Γ , see Equation (3).

$$\Gamma = d_{\text{swollen}} (n_{\text{swollen}} - n_{\text{solvent}}) (\partial c/\partial n) \quad (3)$$

The ratio $\partial c/\partial n$ relates to changes of the refractive index with polymer concentration in water and is based on values of proteins reported in the literature.^[46,47]

Supporting Information

Supporting Information is available from the Wiley Online Library or from the author.

Acknowledgements

This project had received funding from the European Union's Horizon 2020 Research and Innovation Program under grant agreement No

633937, project ULTRAPLACAD. Further, the authors thank for the financial support through the BMBF funded Project Medistorplast (13GW0349C) for FD, from Austrian Science Fund (FWF) via the project DIPLAB I 5119-B for SH, MP, and JD, and from Czech Science Fund (GACR) project APLOMA (22-30456J) for JD.

Open access funding enabled and organized by Projekt DEAL.

Conflict of Interest

The authors declare no conflict of interest.

Data Availability Statement

The data that support the findings of this study are available from the corresponding author upon reasonable request.

Keywords

antifouling thermoresponsive hydrogel coatings, betaines, blood plasma, photocrosslinkable poly(2-oxazoline)s, SPR/OWS

Received: September 12, 2023

Revised: November 3, 2023

Published online:

- [1] I. Banerjee, R. C. Pangule, R. S. Kane, *Adv. Mater.* **2011**, *23*, 690.
- [2] J. B. Kristensen, R. L. Meyer, B. S. Laursen, S. Shipovskov, F. Besenbacher, C. H. Poulsen, *Biotechnol. Adv.* **2008**, *26*, 471.
- [3] B. Liu, X. Liu, S. Shi, R. Huang, R. Su, W. Qi, Z. He, *Acta Biomater.* **2016**, *40*, 100.
- [4] Y.-N. Chou, F. Sun, H.-C. Hung, P. Jain, A. Sinclair, P. Zhang, T. Bai, Y. Chang, T.-C. Wen, Q. Yu, S. Jiang, *Acta Biomater.* **2016**, *40*, 31.
- [5] S. Chen, L. Li, C. Zhao, J. Zheng, *Polymer (Guildf)* **2010**, *51*, 5283.
- [6] J. M. Harris, in *Poly(Ethylene Glycol) Chemistry* (Ed.: J. M. Harris), Springer Science+Business Media, New York **1992**, pp. 1–14.
- [7] Q. Shao, S. Jiang, *Adv. Mater.* **2015**, *27*, 15.
- [8] X. Liu, R. Huang, R. Su, W. Qi, L. Wang, Z. He, *ACS Appl. Mater. Interfaces* **2014**, *6*, 13034.
- [9] T. Goda, M. Tabata, M. Sanjoh, M. Uchimura, Y. Iwasaki, Y. Miyahara, *Chem. Commun.* **2013**, *49*, 8683.
- [10] F. Wang, H. Zhang, B. Yu, S. Wang, Y. Shen, H. Cong, *Prog. Org. Coat.* **2020**, *147*, 105860.
- [11] R. A. Wolf, in *Proc. J. Vinyl and Additive Technology*, Vol. **13**, **2007**, pp. 87–90.
- [12] G. Gunkel, M. Weinhart, T. Becherer, R. Haag, W. T. S. Huck, *Biomacromolecules* **2011**, *12*, 4169.
- [13] B. Liu, X. Liu, S.e Shi, R. Huang, R. Su, W. Qi, Z. He, *Acta Biomater.* **2016**, *40*, 100.
- [14] D. Kuckling, M. E. Harmon, C. W. Frank, *Macromolecules* **2002**, *35*, 6377.
- [15] P. W. Beines, I. Klosterkamp, B. Menges, U. Jonas, W. Knoll, *Langmuir* **2007**, *23*, 2231.
- [16] C. Haslinger, A. Zahoranová, S. Baudis, *Monatsh. Chem.* **2023**, *154*, 459.
- [17] L. Korchia, C. Bouilhac, V. Lapinte, C. Travelet, R. Borsali, J.-J. Robin, *Polym. Chem.* **2015**, *6*, 6029.
- [18] R. Navarro, M. Pérez Perrino, O. Prucker, J. Rühle, *Langmuir* **2013**, *29*, 10932.
- [19] K. Schuh, O. Prucker, J. Rühle, *Macromolecules* **2008**, *41*, 9284.
- [20] R. Hoogenboom, H. Schlaad, *Polymers* **2011**, *3*, 467.

- [21] R. Hoogenboom, *Angew. Chem., Int. Ed.* **2009**, *48*, 7978.
- [22] R. Hoogenboom, H. M. L. Thijs, M. J. H. C. Jochems, B. M. Van Lankvelt, M. W. M. Fijten, U. S. Schubert, *Chem. Commun.* **2008**, 5758.
- [23] F. Diehl, S. Hageneder, S. Fossati, S. K. Auer, J. Dostalek, U. Jonas, *Chem. Soc. Rev.* **2022**, *51*, 3926.
- [24] D. Kotlarek, S. Fossati, P. Venugopalan, N. Gisbert Quilis, J. Slabý, J. Homola, M. Lequeux, F. Amiard, M. Lamy De La Chapelle, U. Jonas, J. Dostálek, *Nanoscale* **2020**, *12*, 9756.
- [25] K. Sergelen, C. Petri, U. Jonas, J. Dostalek, *Biointerphases* **2017**, *12*, 051002.
- [26] M. Toma, U. Jonas, A. Mateescu, W. Knoll, J. Dostalek, *J. Phys. Chem. C* **2013**, *117*, 11705.
- [27] N. Gisbert Quilis, M. Van Dongen, P. Venugopalan, D. Kotlarek, C. Petri, A. Moreno Cencerrado, S. Stanesco, J. L. Toca Herrera, U. Jonas, M. Möller, A. Mourran, J. Dostalek, *Adv. Opt. Mater.* **2019**, *7*, 1900342.
- [28] S. K. Auer, S. Fossati, Y. Morozov, U. Jonas, J. Dostálek, *J. Phys. Chem. B* **2022**, *126*, 3170.
- [29] S. Hageneder, V. Jungbluth, R. Soldo, C. Petri, M. Pertiller, M. Kreivi, A. Weinhäusel, U. Jonas, J. Dostalek, *ACS Appl. Mater. Interfaces* **2021**, *13*, 27645.
- [30] T. R. Dargaville, R. Forster, B. L. Farrugia, K. Kempe, L. Voorhaar, U. S. Schubert, R. Hoogenboom, *Macromol. Rapid Commun.* **2012**, *33*, 1695.
- [31] A. Gress, A. Völkel, H. Schlaad, *Macromolecules* **2007**, *40*, 7928.
- [32] N. Jung, F. Diehl, U. Jonas, *Polymers* **2020**, *12*, 1767.
- [33] L. Korchia, C. Bouilhac, V. Lapinte, C. Travelet, R. Borsali, J.-J. Robin, *Polym. Chem.* **2015**, *6*, 6029.
- [34] C. Haslinger, A. Zahoranová, S. Baudis, *Monatsh. Chem.* **2023**, *154*, 459.
- [35] O. Prucker, C. A. Naumann, J. Rühle, W. Knoll, C. W. Frank, *J. Am. Chem. Soc.* **1999**, *121*, 8766.
- [36] A. Mateescu, Y. Wang, J. Dostalek, U. Jonas, *Membranes* **2012**, *2*, 40.
- [37] M. Gianneli, R. F. Roskamp, U. Jonas, B. Loppinet, G. Fytas, W. Knoll, *Soft Matter* **2008**, *4*, 1443.
- [38] J. D. J. S. Samuel, T. Brenner, O. Prucker, M. Grumann, J. Ducree, R. Zengerle, J. Rühle, *Macromol. Chem. Phys.* **2010**, *211*, 195.
- [39] B. L. Rivas, K. E. Geckeler, in *Advances in Polymer Science*, Springer-Verlag, Berlin **1992**, Vol. 102, pp. 171–188.
- [40] V. P. Dhende, S. Samanta, D. M. Jones, I. R. Hardin, J. Locklin, *ACS Appl. Mater. Interfaces* **2011**, *3*, 2830.
- [41] J. C. Kappel, Y. C. Fan, K. S. Lam, *J. Comb. Chem.* **2008**, *10*, 333.
- [42] C. Petri, *Synthesis and Characterization of Novel Photocrosslinkable Poly(2-Oxazoline)-Based Hydrogel Systems for the Application as Biosensor Matrix*. Dissertation, University of Siegen, Siegen **2018**.
- [43] M. M. Ouberai, K. Xu, M. E. Welland, *Biomaterials* **2014**, *35*, 6157.
- [44] A. Aulasevich, R. F. Roskamp, U. Jonas, B. Menges, J. Dostálek, W. Knoll, *Macromol. Rapid Commun.* **2009**, *30*, 872.
- [45] D. E. Aspnes, *Thin Solid Films* **1982**, *89*, 249.
- [46] G. E. Perlmann, L. G. Longworth, *J. Am. Chem. Soc.* **1948**, *70*, 2719.
- [47] E. Stenberg, B. Persson, H. Roos, C. Urbaniczky, *J. Colloid Interface Sci.* **1991**, *143*, 513.
- [48] B. Sudha, R. Kamble, S. Shashikanth, *J. Serb. Chem. Soc.* **2008**, *73*, 261.
- [49] H. Witte, W. Seeliger, *Justus Liebig's Ann. Chem.* **1974**, *1974*, 996.
- [50] T.-X. Lav, P. Lemechko, E. Renard, C. Amiel, V. Langlois, G. Volet, *React. Funct. Polym.* **2013**, *73*, 1001.
- [51] G. Le Fer, C. Amiel, G. Volet, *Eur. Polym. J.* **2015**, *71*, 523.
- [52] N. M. Leonard, J. Brunckova, *J. Org. Chem.* **2011**, *76*, 9169.
- [53] L. Tauhardt, D. Pretzel, K. Kempe, M. Gottschaldt, D. Pohlert, U. S. Schubert, *Polym. Chem.* **2014**, *5*, 5751.
- [54] J. Seuring, S. Agarwal, *ACS Macro Lett.* **2013**, *2*, 597.
- [55] R. Hoogenboom, H. M. L. Thijs, M. J. H. C. Jochems, B. M. Van Lankvelt, M. W. M. Fijten, U. S. Schubert, *Chem. Commun.* **2008**, 5758.
- [56] A. Laschewsky, *Polymers* **2014**, *6*, 1544.
- [57] R. J. Young, P. A. Lovell, *Introduction to Polymers*, 3rd ed., CRC Press, Boca Raton, FL **2011**.
- [58] M. Namazian, S. Halvani, M. R. Noorbala, *J. Mol. Struct.* **2004**, *711*, 13.
- [59] L. Wu, J. Jasinski, S. Krishnan, *J. Appl. Polym. Sci.* **2012**, *124*, 2154.
- [60] R. R. Netz, D. Andelman, *Phys. Rep.* **2003**, *380*, 1.
- [61] N. Giovambattista, P. G. Debenedetti, P. J. Rossky, *J. Phys. Chem. B* **2007**, *111*, 9581.
- [62] R. J. Scott, L.-Y. Lian, S. H. Muharram, A. Cockayne, S. J. Wood, B. W. Bycroft, P. Williams, W. C. Chan, *Bioorg. Med. Chem. Lett.* **2003**, *13*, 2449.
- [63] S. Sakakibara, N. Inukai, *Bull. Chem. Soc. Jpn.* **1965**, *38*, 1979.
- [64] M. T. Zarka, O. Nuyken, R. Weberskirch, *Chem. - Eur. J.* **2003**, *9*, 3228.
- [65] S. M. Andreev, L. A. Pavlova, Y. A. Davidovich, S. V. Rogozhin, *Russ. Chem. Bull.* **1980**, *29*, 785.
- [66] S. Asano, J. Gavriljuk, D. R. Burton, C. F. Barbas, *ACS Med. Chem. Lett.* **2014**, *5*, 133.
- [67] O. Norberg, L. Deng, M. Yan, O. Ramström, *Bioconjugate Chem.* **2009**, *20*, 2364.
- [68] E. W. Della, P. A. Smith, *J. Org. Chem.* **1999**, *64*, 1798.